One Earth

Article

Modeling atmospheric microplastic cycle by GEOS-Chem: An optimized estimation by a global dataset suggests likely 50 times lower ocean emissions

Graphical abstract

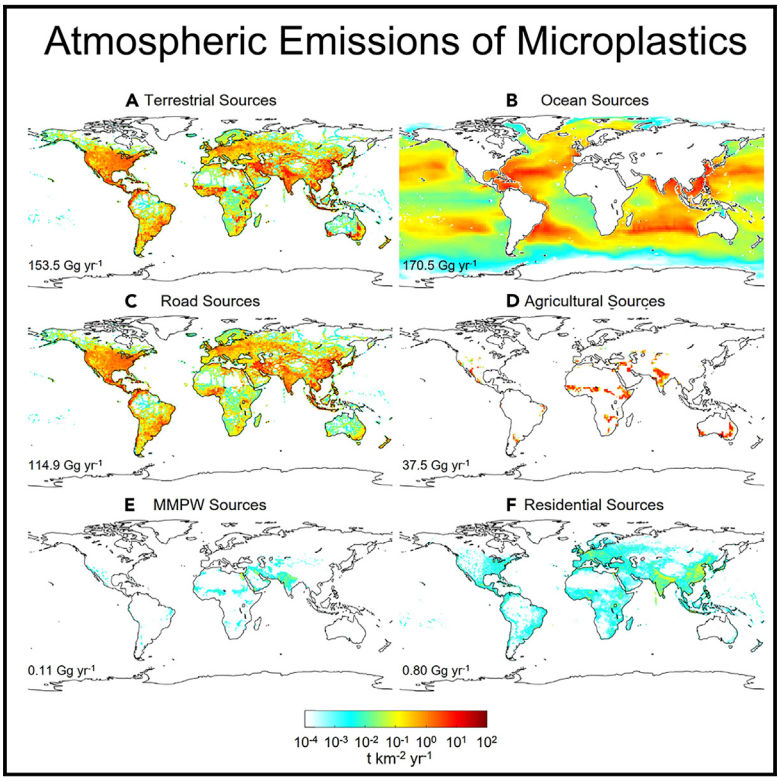

Highlights

- A new atmospheric transport model for microplastics is developed based on GEOS-Chem
- Ocean has a 50 times smaller emission (171 [308–764] Gg year^{-1}) than previously thought
- Almost all (99%) the microplastic particles are emitted as coarse aerosols (70 μm)
- Net land-to-ocean transport is found (25 Gg year^{-1}), much smaller than river discharge

Authors

Yiming Fu, Qiaotong Pang, Suo Lang Zhuo Ga, ..., Xiaohui Wang, Daoji Li, Yanxu Zhang

Correspondence

zhangyx@nju.edu.cn

In brief

The atmosphere plays a crucial role in the microplastic environmental cycle, with its sources still largely unclear. The ocean has been suggested to be the major contributor. In this study, we devise a novel model for atmospheric microplastics, constraining sources using global atmospheric microplastic abundance data. Our findings indicate that ocean emissions are 50 times lower than previously estimated. This underscores the importance of addressing land-based sources, particularly by regulating littering and managing plastic waste disposal near roadways.

Fu et al., 2023, One Earth 6, 705–714
June 16, 2023
https://doi.org/10.1016/j.oneear.2023.05.012

CellPress

One Earth

CellPress

Article

Modeling atmospheric microplastic cycle by GEOS-Chem: An optimized estimation by a global dataset suggests likely 50 times lower ocean emissions

Yiming Fu,[1,5] Qiaotong Pang,[1,5] Suo Lang Zhuo Ga,[1] Peipei Wu,[1] Yujuan Wang,[1] Mao Mao,[1] Zhen Yuan,[2] Xiangrong Xu,[2] Kai Liu,[3] Xiaohui Wang,[3] Daoji Li,[3] and Yanxu Zhang[1,4,6,*]

[1]School of Atmospheric Sciences, Nanjing University, Nanjing 210023, China

[2]Key Laboratory of Tropical Marine Bio-resources and Ecology, Guangdong Provincial Key Laboratory of Applied Marine Biology, South China Sea Institute of Oceanology, Chinese Academy of Sciences, Guangzhou 510301, China

[3]State Key Laboratory of Estuarine and Coastal Research, East China Normal University, Shanghai 200241, China

[4]Frontiers Science Center for Critical Earth Material Cycling, Nanjing University, Nanjing, Jiangsu, China

[5]These authors contributed equally

[6]Lead contact

*Correspondence: zhangyx@nju.edu.cn

https://doi.org/10.1016/j.oneear.2023.05.012

SCIENCE FOR SOCIETY Microplastics are tiny plastic particles that are widespread in our environment and pose potential risks to ecosystems and human health. The atmosphere plays a vital role in moving microplastics over long distances and continuously engages in exchanges with the land and ocean. However, identifying the sources of atmospheric microplastics remains challenging. Previous research suggested that the ocean is the main source, but our study, which combines global data and atmospheric models, reveals that the ocean contributes less than initially thought. Road-related sources, such as tire and brake wear and poorly managed plastic waste, also contribute significantly. Our findings underscore the necessity of regulating litter and dumping of plastic waste near roads. Further data collection and laboratory research are needed to better understand the atmospheric microplastic cycle.

SUMMARY

The atmosphere plays a vital role in microplastic (MP) transport, facilitating continuous exchanges with land and ocean. However, the sources of atmospheric MP remain unclear. Previous studies suggested that the ocean is the primary source, with global emissions reaching up to 8,600 Gg year^{-1}. Here, we use global atmospheric abundance data, a newly developed atmospheric model, and optimal estimation to constrain the atmospheric sources. We find that the global atmospheric MP emissions are 324 (73–1,450) Gg year^{-1}. The ocean source is estimated to have a much smaller global emission (171 [38–764] Gg year^{-1}] than previously believed, followed by road-related sources (115 [26–513] Gg year^{-1}) including the suspension of tire and brake wears and mismanaged plastic waste. We simulate a net land-to-ocean transport by the atmosphere (25 Gg year^{-1}). This highlights the importance of controlling terrestrial sources, and more data are needed to improve our understanding of the atmospheric MP cycle.

INTRODUCTION

Plastics are durable, versatile, and ubiquitous in modern life. While their global production has increased from 1,700 Gg year^{-1} in 1950 to 367,000 Gg year^{-1} in the 2020s, plastic waste management has not kept up, resulting in more than 40,000–80,000 Gg mismanaged plastic waste (MMPW) globally per year.[1,2] MMPW is defined as the plastic waste not properly recycled, incinerated, or buried in landfills but which enters the environment. MMPW is broken down or disaggregated to much smaller microplastics (MPs) (approximately 1 μm–5 mm) or nanoplastics (typically <1,000 nm),[3] which could cause a long-term ecological impact on both terrestrial and aquatic lives,[4,5] act as a vector for contaminants,[6] and even pose a potential threat to human health.[7]

The atmosphere plays an important role in the transport of plastics in the environment, especially MPs smaller than 70 μm.[8–10] Atmospheric long-range transport has been

suggested as the major pathway of MPs observed in the remote environment such as protected areas of the US,[11] pristine mountain catchments in the French Pyrenees,[12] the Tibetan Plateau,[13] and the polar regions.[14] Records of atmospheric MP levels remain sparse, but limited data suggest that atmospheric deposition rates range from 50 to 700 MP m^{-2} d^{-1} with atmospheric concentrations of 10^{-2} to 10^{1} MP m^{-3}.[15]

Two categories of sources are hypothesized as the major contributors to atmospheric MPs: (1) marine sources, such as aerosolization of marine plastics caused by sea spray, and (2) terrestrial sources, such as the resuspension of road-related plastic particles from tires, brakes, and road surfaces; movement of previously deposited or discharged plastics in soils and agriculture lands; and direct atmospheric emissions from human activities occurring around population centers.[8] While most bottom-up inventories focus on plastic emissions to the total environment, the inverse modeling method is often applied to constrain the atmospheric emissions with observed data. For example, Brahney et al.[8] suggest the current global atmospheric emissions of MPs as 8,600 (0–22,000) Gg $year^{-1}$ mainly from the ocean source, and Long et al.[16] found a large tire dust source (280 Gg yea^{-1}) over the continent of Asia.

Residence time is the average time for MP particles to stay in the atmosphere before their removal by dry and wet deposition, which is calculated as the ratio of its atmospheric abundance to total emission flux. The wet deposition of an MP is similar to other aerosol components such as dust and sea salt,[11] while the size, shape, and chemical compositions are important factors influencing the dry deposition velocity of MP particles. The shapes can be pellets, fibers, and sheets with sizes ranging from 10^{-6} to 10^{-3} m.[15] The density ranges, approximately from 0.9 to 1.4 g cm^{-3}, may have an overall smaller influence on deposition velocity than the other factors. Therefore, aerodynamic diameters are often used, as they are directly associated with the residence time of MPs in the atmosphere. In modeling studies, aerodynamic sizes of different MP particles are considered with a residence time from hours to days.[8,16] Given their importance, the sources of atmospheric MPs and their residence times remain unclear.

This study develops an atmospheric transport model for MPs based on the Goddard Earth Observing System (GEOS)-Chem model to determine the most likely sources and residence time of atmospheric MPs. The global atmospheric MP emissions are determined to be 324 (73–1,450) Gg per year. Marine plastic aerosolization is still considered a significant source, but with considerably lower global emissions (171 [38–764] Gg per year), followed by road-related sources (115 [26–513] Gg per year), which include tire and brake wear suspension and improperly managed plastic waste. The findings reveal a predominantly coarse size distribution for these sources, with almost all (99%) of the MP particles classified as very coarse aerosols (70 μm). We calculate a net land-to-ocean transport of atmospheric MP at 25 Gg per year, a considerably smaller amount than riverine discharge and erosion of coastal waste to the ocean (approximately 1,000 Gg per year). Our findings underscore the necessity of regulating litter and dumping of plastic waste near roads. To enhance our comprehension of the atmospheric MP cycle, more data on atmospheric abundance in unexamined regions and direct measurements of emissions from various source categories are required.

RESULTS AND DISCUSSION

Methods summary

The GEOS-Chem model considers the emissions, transport, and deposition of MPs in the atmosphere and includes six aerosol-like MP tracers with aerodynamic sizes ranging from 0.3 to 70 μm and residence times ranging from 0.04 to 6.5 days following Brahney et al.[8] This size range mainly belongs to MPs with the smallest one to nanoplastics, but we call both MPs for simplicity. We lump all shapes of MP particles into these six bins, as the aerodynamic size is the most important influencing factor for their residence time, and pellets also dominate the air samples among other shapes such as fragments and fibers.[16] Possible sources include aerosolized marine plastic, traffic-related sources, resuspension of MMPW and agricultural plastic waste, and generic sources associated with residential activities. The model results are compared with available observed data for atmospheric MPs (both atmospheric concentrations and deposition fluxes). We adopt an optimal estimation approach following Brahney et al.[8] and Long et al.[16] and incorporate all available observational data over the global land and the ocean environment.[15] Due to the close coupling between emission strength and size distribution (i.e., residence time), they are optimized simultaneously in the optimization procedure (more details in the experimental procedures).

Optimized emissions

We find a global total atmospheric MP emission of 324 Gg $year^{-1}$, with terrestrial and marine sources contributing 154 and 171 Gg $year^{-1}$, respectively (Figure 1). Among the terrestrial sources, the road-related source is dominant (115 Gg $year^{-1}$), followed by agriculture dust (38 Gg $year^{-1}$), residential sources (0.80 Gg $year^{-1}$), and MMPW resuspension (0.11 Gg $year^{-1}$). The spatial pattern of ocean emissions follows that of the modeled surface ocean plastic mass, scaled by the wind speed and sea surface temperature (see experimental procedures).[17] The highest emissions are in the subtropical centers of the five gyres (i.e., North Pacific, South Pacific, North Atlantic, South Atlantic, and the Indian Ocean), where convergent ocean circulation causes an accumulation of floating plastic particles (Figure 1B).[18] Road-related emissions follow that of traffic activities with higher emissions in North America, West Europe, East Asia, and South Asia (Figure 1A). The other three categories have much smaller emissions compared with these two.

The optimizer can also infer the size distribution of emissions. The GEOS-Chem model simulates the mass concentrations of six MP bins that have distinct atmospheric residence times. A unit mass of emissions with different sizes thus has different travel distances and a varied impact on the MP concentrations at receptors. By searching within the possible combinations for the size distributions of emissions to minimize the model-observation difference, the optimizer suggests that almost all (99% in mass) MP particles are emitted as very coarse aerosols (70 μm), reflecting the fact that most of them are from the ocean and road-related sources. The fractions from smaller sizes (0.3–35 μm) are much smaller, with negligible contributions. Indeed, these sources are related to mechanical processes forced by strong wind events or wind/wave breaking of sea surface spray. The size distribution of emissions reflects the influence of inertial or cohesive

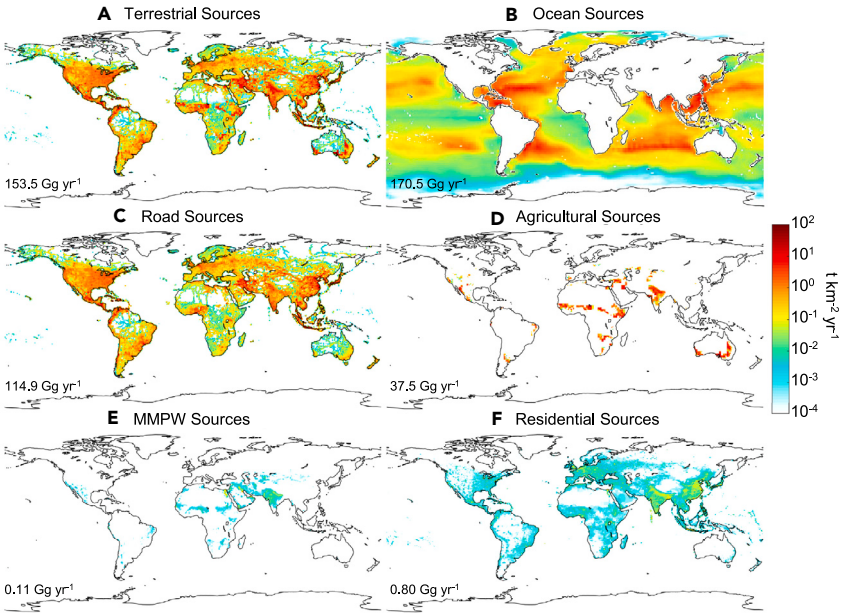

Figure 1. Optimized emissions from a variety of sources

(A) Total terrestrial sources.
(B) Ocean sources.
(C) Road sources.
(D) Agricultural sources.
(E) Mismanaged plastic waste sources.
(F) Residential sources.
Note that the (A) is the sum of (C)–(F), and the color is in a base 10 logarithm scale.

forces on roadside and ocean surfaces. The results are also consistent with observed size distributions of MPs in the marine atmospheric boundary layer (MABL or MBL), with mass concentrations often dominated by sizes >50 μm.[19,20] This size distribution pattern contrasts with combustion processes, which are typically associated with smaller or finer particles like sulfate and black carbon. The residential sources indeed may have a smaller particle size, but our study could not sufficiently constrain it due to the very low overall global emissions. This is generally consistent with previous studies.[8,16] For example, Brahney et al.[8] considered three cases with different prescribed size distributions and found that the best case has 85% global ocean emissions in the 70 μm bin. Long et al.[16] also found that 87% terrestrial emissions and 90% ocean emissions are larger than 50 μm. One drawback of this study is that we use only bulk mass concentrations of observed MPs in the cost function of our optimizer (see experimental procedures), as many studies did not report size distributions or used inconsistent definition of size categories.[9] In addition, many of these studies adopted Fourier transform infrared spectroscopy to identify polymers. This technique is typically limited to size ranges greater than ~30 μm, which thus causes an underestimation of MP particles smaller than this size.[21] Nevertheless, our optimizer can greatly benefit from more consistent observations with detailed size distributions by using a cost function considering such information.

Terrestrial sources

We find a global terrestrial emission source of 154 Gg year^{-1}. Figure 2 compares the model results driven by the optimized emission inventory against these observations. These data include atmospheric deposition fluxes for US national parks and European and Asian coastal cities. Overall, the modeled average deposition flux over all the sites is 3.6 ± 3.8 kg km^{-2} year^{-1}, which is not significantly different from the observations (3.5 ± 3.2 kg km^{-2} year^{-1}) (Figures 2C and 2D). The measured atmospheric deposition flux over US national parks (2.8 ± 2.3 kg km^{-2} year^{-1}), which are remote and mountainous regions, is slightly lower than the data over urban areas in Asia (3.5 ± 2.8 kg km^{-2} year^{-1}). Our model simulates a lower deposition flux of 1.5 ± 1.2 kg km^{-2} year^{-1} in US national parks but at a comparable level (3.9 ± 2.3 kg km^{-2} year^{-1}) over Asia. The model (14 ± 15 ng m^{-3}) also reproduces the observed (18 ± 24 ng m^{-3}) atmospheric MP concentrations over land-based sites. Indeed, our model cannot fully simulate the variability in the observations (e.g., Figure 2D). The optimized terrestrial emission and model performance are similar to those of Brahney et al.[8] (183 Gg year^{-1}), even though we include observations not only over US national parks, which were used by that study, but also data from other continents including atmospheric concentrations and deposition fluxes. This, on one hand, suggests that our estimate for terrestrial sources is quite robust, i.e., not sensitive to a specific subset of data. On the other hand, this may mean that both our optimized results are local optimums due to the lack of size distribution information, which is the key to further improve the model performance.

The optimized results suggest that road-related (115 Gg year^{-1}) and agricultural (38 Gg year^{-1}) sources contribute the most to total terrestrial emissions, while the contributions from MMPW and residential sectors are much smaller. This is generally consistent with Brahney et al.[8] and Long et al.,[16] but we estimate a lower emission from agricultural sources than Brahney et al.[8] (69 Gg year^{-1}). We scale the MP emissions of this source by the fraction of agricultural land use and dust emission fluxes, which are quite sporadic but had no observations available nearby (see experimental procedures; Figure 1C). We thus call for more observations near these source regions to better constrain this source. The residential sector contains sources that include synthetic fibers from clothing, artificial turf, personal care, and cosmetic products.[22] We scale the spatial pattern of this source by population density following Brahney et al.[8] We find that the relatively high MP deposition flux over US national parks with low population density drives down the optimized emission for this category.

It is surprising to find that the aerosolization of MMPW is a negligible source. MMPW emissions are based on MMPW generation (see experimental procedures), which has a larger emission from populous developing countries such as India and China (Figure 1E).[1] Wind speed and soil moisture also influence the emissions analogous to dust emissions, which makes higher emissions over dry and windy climate regions such as the Middle East

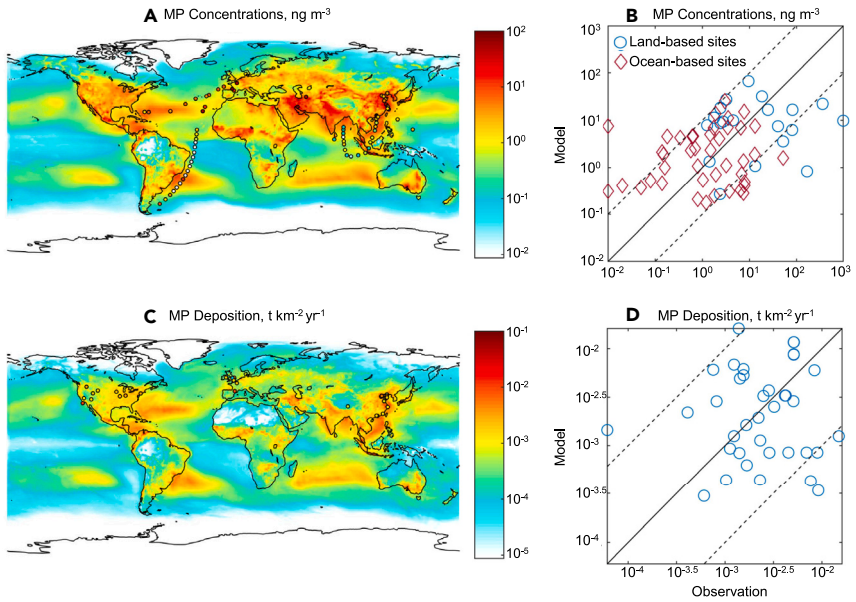

Figure 2. Comparison of model results driven by optimized emissions against observations

(A and B) Atmospheric MP concentrations at ground level.

(C and D) Atmospheric MP depositions.

Note that the colors in (A) and (C) and the axes of (B) and (D) are in a base 10 logarithm scale.

(Figure 1D). Developed countries in Western Europe and North America have generally lower MMPW emissions due to better waste management practices.[1,23] However, such a pattern is not well supported by the available observation data, and the optimizer generates a low weighting factor for this source category.

An alternative explanation is that the optimized road-related source does not only include plastic emissions from tire and brake wears but also the aerosolization of MMPW dumped and/or littered roadside, which consists of two-thirds of all MMPW.[24] Exposure to the environment including ultra-violet radiation, high temperatures, and being smashed by vehicles further break it down into microscopic fragments before being brought into the atmosphere by the energetic flows and turbulence caused by traffic.[8] This is also supported by the fact that road dust consists of multiple chemical compositions rather than just tire materials (natural or synthetic rubber).[25] Atmospheric MP samples across different environments are also often identified mainly as polystyrene (PS), polyethylene terephthalate (PET), polypropylene (PP), polyethylene (PE), and nylon, which are the major chemical components of MMPW.[9,11,26] The amount of MMPW generation seems not to be a limiting factor for its source in the atmosphere but is driven by aerosolization related to traffic activities. This also implies the importance of controlling the littering and dumping of plastic waste in the near-road environment.

Marine sources

We find much lower emissions from ocean sources (171 Gg year^{-1}) compared with previous studies, e.g., 8,600 Gg year^{-1} by Brahney et al.[8] Long et al.[16] calculated an ocean source of 60 Gg year^{-1} for the western Pacific and Indian Oceans, which can be scaled to a global emission of 1,500 Gg year^{-1} following the spatial pattern of ocean emissions simulated by Brahney et al.[8] These differences can be first attributed to the different observation datasets. Indeed, Brahney et al.[8] derived the ocean emissions based on inland observations at US national parks, with an extremely low contribution of oceanic sources at these sites. Their estimation thus carries a large uncertainty range of 0–22,000 Gg year^{-1}. By including observations in the MBL of the Pacific and the Indian Ocean, the magnitude of the ocean source is drawn down greatly by Long et al.[16] and this study. Indeed, the much lower measured atmospheric MP concentrations in the MBL (4.1 ± 8.3 ng m^{-3}) than in the land-based sites (18 ± 24 ng m^{-3}) suggest a relatively low ocean emission. Our model well reproduces this land-ocean gradient (3.7 ± 5.1 vs. 14 ± 15 ng m^{-3}) (Figures 2A and 2B).

Another cause of the difference is the spatial distribution of ocean emissions, which is calculated based on the surface ocean plastic mass concentrations and the sea salt emission fluxes in this and previous studies.[8,16] While the sea salt emissions are calculated by similar methods (as a function of sea surface temperature and wind speed; see experimental procedures for details), different assumptions are used for the surface ocean plastic abundance. Brahney et al.[8] used the surface ocean flow convergence as a proxy for the plastic abundance in the surface ocean. However, they ignored the spatial distribution of marine plastic emissions (including riverine and coastal sources[23,27]) and their transport pattern to the centers of ocean gyres.[28] Long et al.[16] improved this by using a global inventory of floating plastic particles based on observed surface ocean abundance data interpreted by plastic trajectory models.[28] However, these models represent plastics as virtual tracers without considering the actual fragmentation, degradation, sinking, and biofouling processes.[29] In this study, we use the results of a Euler model that takes into account the actual transport and biogeochemical processes of plastic particles in the seawaters, driven by actual riverine and coastal plastic emission inventories (Figure S1).[30] Compared with previous results,[28] this model generally captures the spatial variability of observed ocean plastic concentrations in the whole water column and is quantitatively linked to riverine and coastal sources.[30] Indeed, the absolute magnitude of the simulated plastic concentrations is subjected to large uncertainty due to the large variability of the model parameters, but the relative spatial distribution is expected to be much more robust.[30]

There is generally a paucity of atmospheric MP observations over the MBL, except for a few cruises in the western Pacific, Indian, and Atlantic Oceans (Figure 3A).[15] Existing MBL studies may suffer from low sample volumes and low particle counts on filters due to logistical and technical reasons (e.g., a sampler with a flow rate of ~20 L/min used by Trainic et al.[31]), limiting

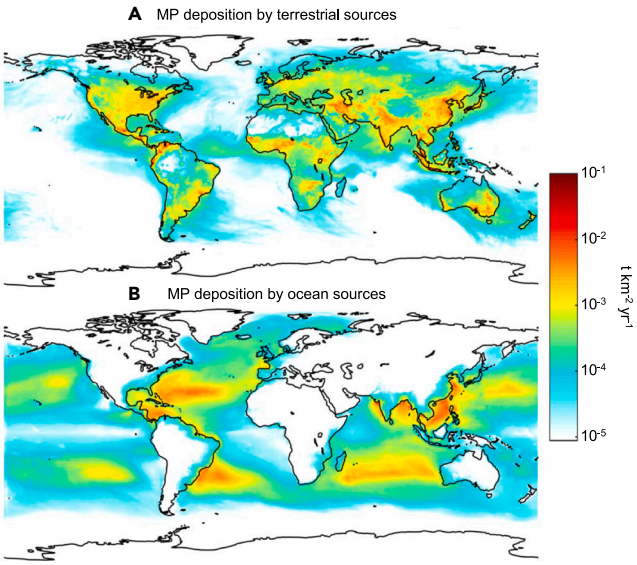

Figure 3. Total deposition contributed by different sources
(A) Terrestrial sources.
(B) Marine sources.
Note that the colors are in a base 10 logarithm scale.

the comparability with land-based studies, which often have higher sampling volumes and lower limits of detection.[15] However, we find that our optimized ocean emissions are rather robust without being sensitive to individual studies. For example, removing the Trainic dataset in the North Atlantic Ocean has no significant impact on our optimized results. The overall agreement with the MBL dataset also indicates that our model captures the large-scale variability of ocean MP emissions (Figures 2A and 2B), which lends confidence to this dataset in revealing the relative spatial pattern of atmospheric MP abundance.

Other approaches to determine the magnitude of ocean MP emissions include either *in situ* or laboratory flux measurements. The former remains lacking in the literature, while the latter suggests much lower ocean emissions than previous estimates. For example, a recent study by Yang et al.[32] estimated global ocean MP emissions to be less than 1 Gg year^{-1} based on the sea salt aerosol generation tank method. Although such a laboratory study cannot represent the full dynamic range of realistic wind speeds and subsequent wave and bubbling conditions, the generally low MP emission factor with regard to sea salt aerosol supports the findings of our results. Despite our initial effort to include MBL MP data in an inverse analysis, further observations and a more comprehensive approach are needed to better constrain this source. In particular, more consistent sampling and analyzing techniques are required, along with more *in-situ*- or laboratory-based flux measurements under more realistic oceanic conditions. Additionally, it is necessary to gather more data on the abundance of atmospheric plastics in the MBL over garbage patches in the centers of gyres, such as the Great Pacific Garbage Patch.[33]

Land-ocean transport

Figure 3 shows the spatial distribution of atmospheric deposition fluxes contributed by terrestrial and marine sources, totaling 152 and 170 Gg year^{-1}, respectively, a slight discrepancy from the emissions due to the seasonal variation in atmospheric plastic abundance. The spatial pattern of deposition largely resembles that of the emissions due to the relatively short residence time of the coarse plastic particles. Indeed, the average lifetime of a plastic particle with an aerodynamic size of 70 μm is approximately 1 h and has a short travel distance (<100 km) given a wind speed of 10 m s^{-1}.[16] The deposition flux of terrestrial sources to the global ocean is 32 Gg yr^{-1}, and the marine sources to land are 8.2 Gg yr^{-1}, both are rather limited to the coastal regions (Figure 3). This results in a net land-to-ocean transport of 25 Gg year^{-1} that is consistent with Long et al.[16] but contradicts Brahney et al.,[8] as the latter suggests a net ocean-to-land transport (9 Gg year^{-1}) because of its high ocean emissions. The net land-to-ocean transport is confirmed by the higher offshore atmospheric MP concentrations than the pelagic areas.[34] It is also not against our intuition, as terrestrial sources are the ultimate source of plastics in the environment. This indicates that riverine and coastal discharges are the major pathways for plastics entering the marine environment (4,000–13,000 Gg year^{-1}),[23,35] dwarfing the atmospheric transport and deposition (25 Gg year^{-1}).

Figure 4 shows a budget for atmospheric MPs. The simulated total atmospheric MP mass is 0.60 Gg with an overall lifetime against deposition of 0.68 days. This is also consistent with previous estimates for the MPs from terrestrial and marine sources (0.10–0.62 days).[8] The atmospheric lifetime of an MP is determined to be relatively short, which limits its long-range transport potential.[16] This also implies that the air-sea exchange and atmospheric transport may not be able to significantly redistribute the MP in the surface ocean. Indeed, we may underestimate such potential, as currently available observations only include MPs >4 μm, while fine particles, especially nanoplastic particles, are known to be able to transport across continents.[36]

Uncertainty analysis

We first estimate the uncertainty by a "leave-one-out" approach, i.e., alternatively drop an observation data point for the optimizer, as the number of observational data is relatively small. This results in relatively small interquartile ranges of 168–172, 32–48, and 103–110 Gg year^{-1} for the ocean, agricultural, and road sources, respectively (Figure 5), indicating the robustness of the optimizer. The uncertainty of our optimized emissions can also be represented by the discrepancy between model and observed values, as all the MP emission, transport, and deposition processes are linear. The root-mean-squared errors are 0.65 and 0.37 orders of magnitude for the MP concentrations and depositions, respectively (Figure 2B and 2D). Using the larger one for a conservative estimation, we can deduce that our optimized emissions also vary by a 0.65 order of magnitude. This results in uncertainty ranges of 154 (34–688) and 171 (38–764) Gg year^{-1} for terrestrial and marine sources, respectively, and 324 (73–1,450) Gg year^{-1} for total emissions.

The optimizer uses the spatial patterns of different emission sources as a fingerprint, adjusting their emission strength and size distributions to best match the available observations. More observations covering the complete spatial features of different sources are thus of vital importance (e.g., garbage patches for ocean emissions). Furthermore, uncertainties are introduced when proxies are used for the source spatial

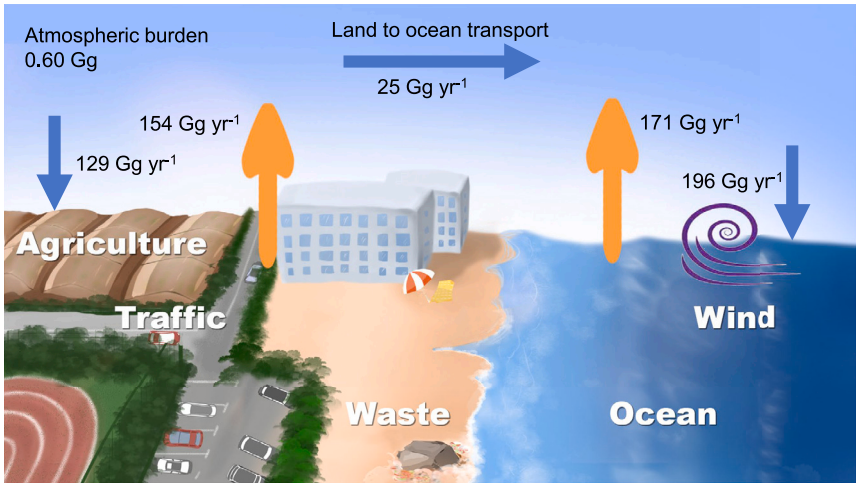

Figure 4. A global budget of atmospheric microplastics
Vertical arrows indicate different emission sources with horizontal ones as transport between the atmosphere and ocean.

distributions, e.g., traffic emissions of NO for traffic activities and sea salt spray for ocean plastic aerosolization (see experimental procedures). In addition, our optimizer cannot provide an effective constraint on the nanoplastics as none of the observations include such small size ranges. Our model framework also does not consider the fragmentation and decomposition of MPs by physical and microbial processes, which are important sources of nanoplastics. This limits the environmental implications of our study.

Understanding and modeling atmospheric MP cycles are still in their embryo stage. Our study develops a new global model for their atmospheric transport and deposition. Incorporating a global dataset and using different spatial surrogates for candidate emission sources also generate a different budget of atmospheric MPs compared with previous studies, which also demonstrates the uncertainty of our understanding of the key processes of atmospheric MP cycles. More atmospheric abundance data, especially over the unsampled areas (e.g., the Southern Hemisphere and garbage patches in the center of gyres), and direct measurements of the strength, size distribution (including nanoplastics), chemical composition, and morphological features of different source categories (i.e., a bottom-up approach, e.g., for oceanic, road, MMPW resuspension, and agricultural sources) are needed to evolve our understanding the atmospheric MP cycles.

EXPERIMENTAL PROCEDURES

Resource availability

Lead contact

Further information and requests for resources and reagents should be directed to and will be fulfilled by the lead contact, Yanxu Zhang (zhangyx@nju.edu.cn).

Materials availability

This study did not generate new unique materials.

Data and code availability

The GEOS-Chem code is available at https://www.geos-chem.seas.harvard.edu. Other code and datasets have been deposited at Mendeley Data (https://doi.org/10.17632/52knh3btb3.1). Any additional information required to reanalyze the data reported in this paper is available from the lead contact upon request.

GC-MP model

The global three-dimensional GEOS-Chem v.14.1.1 is adopted to simulate the atmospheric emission, transport, and deposition of MPs. The model is run with a 0.5° latitude × 0.625° longitude horizontal resolution and 72 vertical layers extending to 0.01 hPa. The model is driven by meteorological data from the GEOS (https://gmao.gsfc.nasa.gov/GMAO_products/NRT_products.php). MERRA-2 reanalysis data with a native resolution of 0.5° latitude × 0.625° longitude and 72 levels is used. We run the model for the year 2018–2020 with a spin-up time of 2 months. The model is run in an aerosol-only model including aerosols of anthropogenic and natural sources (sulfate, nitrate, ammonium, carbonaceous, dust, and sea salt) with archived gaseous phase chemical tracers.[37] The MPs are added to the GEOS-Chem aerosol-only simulation as insoluble aerosol tracers with six different aerodynamic diameters (0.3, 2.5, 7, 15, 35, and 70 μm) following Brahney et al.[8] (referred to as GC-MP). As the density of plastics is much larger than the air, we use a uniform 1 g cm^{-3} for all particles.[8] The model uses the TPCORE advection algorithm of Lin and Rood,[38] and convective transport is computed from the convective mass fluxes in the meteorological archive as described by Wu et al.[39] Boundary layer mixing uses the non-local scheme implemented by Lin and McElroy.[40] The wet deposition scheme is described by Liu et al.[41] for water-soluble aerosols. Scavenging of aerosols by snow and cold/mixed precipitation follows Wang et al.[42,43] Dry deposition is based on the resistance-in-series scheme of Wesely.[44] Size-dependent aerosol dry deposition is from Emerson et al.[45] with gravitational deposition following Fairlie et al.[46] for dust and Alexander et al.[47] and Jaeglé et al.[17] for sea salt.

MP emissions

Several emission source candidates are considered in this study, including aerosolized marine plastic, traffic-related sources, deflation of MMPW and agricultural plastic waste, and generic sources associated with domestic activities largely following Brahney et al.[8] An extension based on the HEMCO 3.0 facility is developed for these MP sources in the GC-MP model. The emissions of these sources change dynamically at each model time step depending on meteorological factors or scaled by the emissions of other species.[48]

The ocean emission flux density of MP (F_{ocean}) is simulated based on the ocean surface plastic concentrations (C_{MP}) scaled by the emission flux of sea salt spray ($F_{seasalt}$). The sea salt emission is calculated based on wind speed and sea surface temperature following Jaeglé et al.[17] (Equations 1 and 2):

$$F_{ocean} = k_{ocean} \times C_{MP} \times F_{seasalt}, \text{ and} \quad \text{(Equation 1)}$$

$$F_{seasalt} = (0.329 + 0.0904T - 0.00717T^2 + 0.00027T^3) \times U_{10m}^{3.41}, \quad \text{(Equation 2)}$$

where k_{ocean} is a scalable parameter adjusted by the optimizer (elaborated below), T is the sea surface temperature, and U_{10m} is the wind speed at 10 m height.

The ocean surface plastic concentrations are taken from the model output of the NJU-MP model, which is a Euler-based three-dimensional global ocean plastic model as described by Peng et al.[18] and Zhang et al.[30] This model considers the emissions, windage, ocean transport, and sinking of plastic tracers with different sizes, chemical components, and densities in the ocean. The fragmentation, degradation, biofouling/defouling, beaching, and sedimentation processes of plastic processes are also considered with constraints

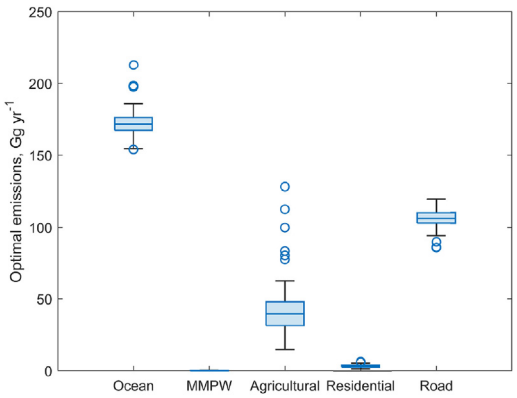

Figure 5. Uncertainty of optimal emissions from a variety of sources calculated by "leave-one-out" strategy

The top and bottom edges of the boxes represent 75% and 25% percentiles, respectively, with horizontal line inside the box as median. The whiskers are the non-outlier maximum and minimum, with circles as outliers.

from available surface ocean plastic concentrations. The model is driven by historical emissions from rivers, coastal zones, and direct ocean dumping from 1950 to 2018 scaled by accumulated plastic production and shipping/fishing activities.[18] The model simulates different plastic types such as PE, PP, polyvinyl chloride, PS, and acrylonitrile butadiene styrene, which are divided into four MP (<0.0781, 0.0781–0.3125, 0.3125–1.25, and 1.25–5 mm) and two macroplastic bins (5–50 and >50 mm). Due to the model uncertainties in the plastic fragmentation process,[30] this study uses the annual total plastic concentrations from all bins in the surface ocean for the final simulation year (2018) as a surrogate for the potential of atmospheric MP emissions.

The direct emission of MMPW (F_{MMPW}) is simulated based on the MMPW generation flux (E_{MMPW}) scaled by wind speed analog to dust aerosols[49] (Equation 3):

$$F_{MMPW} = \begin{cases} k_{MMPW} \times E_{MMPW} \times U_{10m}^2 \times (U_{10m} - U_{th}) & , U_{10m} > U_{th} \\ 0 & , U_{10m} < U_{th} \end{cases}, \quad \text{(Equation 3)}$$

where k_{MMPW} is a scalable parameter adjusted by the optimizer and U_{th} is a threshold wind speed calculated as a function of MP size (d_{MP}), density (ρ_{MP}), and soil moisture (θ) (Equations 4, 5, 6, and 7):

$$U_{th} = 1.29 \times 10^{-3} \times (1.2 + 0.2 \log_{10} \theta) \times \sqrt{\frac{\alpha \times \beta}{\gamma}}, \quad \text{(Equation 4)}$$

$$\alpha = \frac{\rho_{MP} \times g \times d_{MP}}{\rho_{air}}, \quad \text{(Equation 5)}$$

$$\beta = 1 + \frac{0.006}{\rho_{MP} \times g \times d_{MP}^{2.5}}, \quad \text{(Equation 6)}$$

$$\gamma = 1.928 Re^{0.092} - 1, \quad \text{(Equation 7)}$$

where g is the gravity acceleration, ρ_{air} is the density for air, and Re is the Reynold number (Equation 8):

$$Re = 1331 \times d_{MP}^{1.56} + 0.38. \quad \text{(Equation 8)}$$

The release of MMPW to the total environment (E_{MMPW}) is from Borrelle et al.,[1] which is estimated based on the population, waste generation, and waste management levels of different countries. This dataset provides the total MMPW generation of each country, and we interpolate it to the model grids within each country using the gridded population density as a spatial proxy (https://sedac.ciesin.columbia.edu/data/set/gpw-v4-population-density-rev11).

The MP emission from agricultural sources (F_{agri}) is calculated by a similar method to MMPW but scaled by the fraction of agricultural land use in a model grid (f_{agri})[50] (Equation 9):

$$F_{agri} = \begin{cases} k_{agri} \times U_{10m}^2 \times (U_{10m} - U_{th}) \times f_{agri} & , U_{10m} > U_{th} \\ 0 & , U_{10m} < U_{th} \end{cases}. \quad \text{(Equation 9)}$$

We assume that all crop areas have the same fraction of MPs in soil, following Brahney et al.[8] The effect of crop growth is also not considered due to the lack of data.

The generic sources associated with residential activities such as emissions from households (e.g., synthetic fibers from clothing), construction work, artificial turf, and personal care and cosmetic products are scaled by the gridded population density dataset (*POP*) (Equation 10):

$$F_{resi} = k_{resi} \times POP, \quad \text{(Equation 10)}$$

where k_{resi} is an adjustable parameter by the optimizer. The spatial distribution of traffic emissions is assumed to follow that of NO emissions from traffic sources ($E_{traffic}$) based on the CEDS v.2 inventory (https://data.pnnl.gov/dataset/CEDS-4-21-21) (Equation 11):

$$F_{road} = k_{road} \times E_{traffic}^{NO}, \quad \text{(Equation 11)}$$

where k_{road} is a parameter scaled by the optimizer. The traffic NO emissions are used as a spatial proxy for traffic activities including number of vehicles, vehicle speed, type, and loads. This source does not only include road tire and braking emissions but also the aerosolization of MMPW dumped on and/or near roads.

Observational dataset

The global dataset for atmospheric MP abundance compiled by Allen et al.[15] is used in this study. This dataset contains 73 studies published to date, which include air concentration and deposition sampling, and surface sampling potentially representative of atmospheric deposition. We include only outdoor air concentration sampled with a flow rate >1 L/min and direct deposition sampling results. We also include new studies for air concentration and deposition flux data in Guangzhou, China, and the South Atlantic Ocean (concentration only[51,52]). We retain the observations with size ranges >70 μm, as larger sizes often consist of mainly fibers or lines. Although these fibers may be relatively long in their longest dimension, their deposition velocity is shorter than or comparable to pellets with sizes <50 μm.[16] Thus, they can be generally represented by the six tracers in our model that have an aerodynamic size range of 0.3–70 μm. This results in a total of 109 points for our observation dataset, including 72 concentration and 37 deposition points.

We calculate the seasonal mean of observations for the corresponding sampling periods, as many of the observational studies did not report their raw (typically daily) data. We maximize our spatial coverage by sacrificing some temporal resolution but retaining the important seasonal variations. These data are reported as number concentrations (i.e., items per unit volume or per unit area and time). To better compare MP emissions with a mass unit, the reported number concentrations are transferred to a mass unit. The average single-particle mass is assumed to be 57 ng/item for terrestrial samples[11] and 100 ng/item for marine samples.[34]

Optimal estimation

As the magnitudes of the atmospheric MP sources (i.e., F_{ocean}, F_{MMPW}, F_{agri}, F_{resi}, and F_{road}) are generally unknown, and as atmospheric emission inventories are lacking in the literature, we consider only the spatial patterns but leave the magnitudes optimized by observations. We run the GC-MP with individual candidate emission sources alternatively to get the spatial pattern of atmospheric MP abundance. The sensitivity of atmospheric abundance (S^C and S^D for concentrations and depositions, respectively) is also calculated for each model grid to the global emission ($F_{i,j}$) of the source category i = 1, 2, …, 5 (ocean, MMPW, agriculture, residential, and road sources) and size bin j = 1, 2, …, 6 (0.3–70 μm as described above). A cost function (J) is used to represent the deviation of model results from observations (Equation 12):

$$J = \sum_k (\log_{10} C_{model,k} - \log_{10} C_{obs,k})^2 + \sum_l (\log_{10} D_{model,l} - \log_{10} D_{obs,l})^2 + P, \quad \text{(Equation 12)}$$

where k and l represent individual observed air concentration (C) or depositions (D) and the subscript model and obs represent modeled and observed values, respectively. C_{model} and D_{model} are calculated using Equations 13 and 14:

$$C_{model,k} = \sum_i \sum_j S^C_{i,j,k} F_{i,j}, \text{ and} \quad \text{(Equation 13)}$$

$$D_{model,l} = \sum_i \sum_j S^D_{i,j,l} F_{i,j}, \quad \text{(Equation 14)}$$

where k and l represent the model grids the observed concentrations and deposition data fall in, respectively. To consider the seasonal changes in emission and transport conditions, we sample the model at the same month as the observations. For observations outside of the model coverage (i.e., 2018–2020), we use the multiple-year monthly mean. P is a penalty function to make sure we get a positive F (Equation 15):

$$P = 10^5 \times \sum_i \sum_j (|F_{i,j}| - F_{i,j}). \quad \text{(Equation 15)}$$

The minimum of J is found using a gradient descent approach by the fminsearch function provided by the MATLAB software. The state variable is the k values for the five sources (in Equations 1, 3, and 9–11) for all size bins with a degree of freedom of 5 × 6 = 30. The initial conditions of $F_{i,j}$ are taken from Brahney et al.[8]

SUPPLEMENTAL INFORMATION

Supplemental information can be found online at https://doi.org/10.1016/j.oneear.2023.05.012.

ACKNOWLEDGMENTS

We thank Hao Wang for helpful discussions and comments. Y.Z. acknowledges financial support from the National Key R&D Program of China (2019YFA0606803), the Fundamental Research Funds for the Central Universities (0207-14380188 and 0207-14380168), and the Frontiers Science Center for Critical Earth Material Cycling. X.X. acknowledges the financial support of the National Natural Science Foundation of China (41876129 and U2005207). We acknowledge Xin Wang and the other researchers involved in collecting, analyzing, and sharing the atmosphere and ocean MP data.

AUTHOR CONTRIBUTIONS

Y.F., Q.P., S.L.Z.G., and Y.Z. performed the study. Y.Z. designed the study. P.W., Y.W., and M.M. conducted data analyses. Z.Y., X.X., K.L., X.W., and D.L. provided observational datasets. Y.Z. wrote the original draft, with all other authors reviewing and editing.

DECLARATION OF INTERESTS

The authors declare no competing interests.

INCLUSION AND DIVERSITY

We support inclusive, diverse, and equitable conduct of research.

Received: December 7, 2022
Revised: March 28, 2023
Accepted: May 11, 2023
Published: June 16, 2023

REFERENCES

1. Borrelle, S.B., Ringma, J., Law, K.L., Monnahan, C.C., Lebreton, L., McGivern, A., Murphy, E., Jambeck, J., Leonard, G.H., Hilleary, M.A., et al. (2020). Predicted growth in plastic waste exceeds efforts to mitigate plastic pollution. Science *369*, 1515–1518. https://doi.org/10.1126/science.aba3656.
2. Lebreton, L., and Andrady, A. (2019). Future scenarios of global plastic waste generation and disposal. Palgr Commun *5*, 6. https://doi.org/10.1057/s41599-018-0212-7.
3. Huang, D., Tao, J., Cheng, M., Deng, R., Chen, S., Yin, L., and Li, R. (2021). Microplastics and nanoplastics in the environment: macroscopic transport and effects on creatures. J. Hazard Mater. *407*, 124399. https://doi.org/10.1016/j.jhazmat.2020.124399.
4. Wang, W., Gao, H., Jin, S., Li, R., and Na, G. (2019). The ecotoxicological effects of microplastics on aquatic food web, from primary producer to human: a review. Ecotox Environ Safe *173*, 110–117. https://doi.org/10.1016/j.ecoenv.2019.01.113.
5. Chae, Y., and An, Y.J. (2020). Nanoplastic ingestion induces behavioral disorders in terrestrial snails: trophic transfer effects via vascular plants. Environ Sci-Nano *7*, 975–983. https://doi.org/10.1039/c9en01335k.
6. Ziccardi, L.M., Edgington, A., Hentz, K., Kulacki, K.J., and Kane Driscoll, S. (2016). Microplastics as vectors for bioaccumulation of hydrophobic organic chemicals in the marine environment: a state-of-the-science review. Environ. Toxicol. Chem. *35*, 1667–1676. https://doi.org/10.1002/etc.3461.
7. Rubio, L., Marcos, R., and Hernández, A. (2020). Potential adverse health effects of ingested micro- and nanoplastics on humans. Lessons learned from in vivo and in vitro mammalian models. J. Toxicol. Env. Heal. B. *23*, 51–68. https://doi.org/10.1080/10937404.2019.1700598.
8. Brahney, J., Mahowald, N., Prank, M., Cornwell, G., Klimont, Z., Matsui, H., and Prather, K.A. (2021). Constraining the atmospheric limb of the plastic cycle. Proc. Natl. Acad. Sci. USA *118*, e2020719118. https://doi.org/10.1073/pnas.2020719118.
9. Allen, S., Allen, D., Baladima, F., Phoenix, V.R., Thomas, J.L., Le Roux, G., and Sonke, J.E. (2021). Evidence of free tropospheric and long-range transport of microplastic at Pic du Midi Observatory. Nat. Commun. *12*, 7242. https://doi.org/10.1038/s41467-021-27454-7.
10. Sonke, J.E., Koenig, A.M., Yakovenko, N., Hagelskjær, O., Margenat, H., Hansson, S.V., De Vleeschouwer, F., Magand, O., Le Roux, G., and Thomas, J.L. (2022). A mass budget and box model of global plastics cycling, degradation and dispersal in the land-ocean-atmosphere system. Microplast. nanoplast. *2*, 28. https://doi.org/10.1186/s43591-022-00048-w.
11. Brahney, J., Hallerud, M., Heim, E., Hahnenberger, M., and Sukumaran, S. (2020). Plastic rain in protected areas of the United States. Science *368*, 1257–1260. https://doi.org/10.1126/science.aaz5819.
12. Allen, S., Allen, D., Phoenix, V.R., Le Roux, G., Jiménez, P.D., Simonneau, A., Binet, S., and Galop, D. (2019). Atmospheric transport and deposition of microplastics in a remote mountain catchment (vol 12, pg 339, 2019). Nat. Geosci. *12*, 679. https://doi.org/10.1038/s41561-019-0409-4.
13. Dong, H., Wang, L., Wang, X., Xu, L., Chen, M., Gong, P., and Wang, C. (2021). Microplastics in a remote lake basin of the Tibetan plateau: impacts of atmospheric transport and glacial melting. Environ. Sci. Technol. *55*, 12951–12960. https://doi.org/10.1021/acs.est.1c03227.
14. Bergmann, M., Mützel, S., Primpke, S., Tekman, M.B., Trachsel, J., and Gerdts, G. (2019). White and wonderful? Microplastics prevail in snow from the Alps to the Arctic. Sci. Adv. *5*, eaax1157. https://doi.org/10.1126/sciadv.aax1157.
15. Allen, D., Allen, S., Abbasi, S., Baker, A., Bergmann, M., Brahney, J., Butler, T., Duce, R.A., Eckhardt, S., Evangeliou, N., et al. (2022). Microplastics and nanoplastics in the marine-atmosphere environment. Nat. Rev. Earth Environ. *3*, 393–405. https://doi.org/10.1038/s43017-022-00292-x.
16. Long, X., Fu, T.M., Yang, X., Tang, Y., Zheng, Y., Zhu, L., Shen, H., Ye, J., Wang, C., Wang, T., and Li, B. (2022). Efficient atmospheric transport of microplastics over Asia and adjacent oceans. Environ. Sci. Technol. *56*, 6243–6252. https://doi.org/10.1021/acs.est.1c07825.
17. Jaeglé, L., Quinn, P.K., Bates, T.S., Alexander, B., and Lin, J.T. (2011). Global distribution of sea salt aerosols: new constraints from in situ and remote sensing observations. Atmos. Chem. Phys. *11*, 3137–3157. https://doi.org/10.5194/acp-11-3137-2011.

18. Peng, Y., Wu, P., Schartup, A.T., and Zhang, Y. (2021). Plastic waste release caused by COVID-19 and its fate in the global ocean. Proc. Natl. Acad. Sci. USA *118*, e2111530118. https://doi.org/10.1073/pnas.2111530118.

19. Wang, X., Li, C., Liu, K., Zhu, L., Song, Z., and Li, D. (2020). Atmospheric microplastic over the South China sea and East Indian ocean: abundance, distribution and source. J. Hazard Mater. *389*, 121846. https://doi.org/10.1016/j.jhazmat.2019.121846.

20. Ding, Y., Zou, X., Wang, C., Feng, Z., Wang, Y., Fan, Q., and Chen, H. (2021). The abundance and characteristics of atmospheric microplastic deposition in the northwestern South China Sea in the fall. Atmos. Environ. *253*, 118389. https://doi.org/10.1016/j.atmosenv.2021.118389.

21. Allen, S., Allen, D., Moss, K., Le Roux, G., Phoenix, V.R., and Sonke, J.E. (2020). Examination of the ocean as a source for atmospheric microplastics. PLoS One *15*, e0232746. https://doi.org/10.1371/journal.pone.0232746.

22. Wang, T., Li, B., Zou, X., Wang, Y., Li, Y., Xu, Y., Mao, L., Zhang, C., and Yu, W. (2019). Emission of primary microplastics in mainland China: invisible but not negligible. Water Res. *162*, 214–224. https://doi.org/10.1016/j.watres.2019.06.042.

23. Jambeck, J.R., Geyer, R., Wilcox, C., Siegler, T.R., Perryman, M., Andrady, A., Narayan, R., and Law, K.L. (2015). Plastic waste inputs from land into the ocean. Science *347*, 768–771. https://doi.org/10.1126/science.1260352.

24. Kawecki, D., and Nowack, B. (2019). Polymer-specific modeling of the environmental emissions of seven commodity plastics as macro- and microplastics. Environ. Sci. Technol. *53*, 9664–9676. https://doi.org/10.1021/acs.est.9b02900.

25. Dehghani, S., Moore, F., and Akhbarizadeh, R. (2017). Microplastic pollution in deposited urban dust, Tehran metropolis, Iran. Environ. Sci. Pollut. Res. *24*, 20360–20371. https://doi.org/10.1007/s11356-017-9674-1.

26. Dris, R., Gasperi, J., Mirande, C., Mandin, C., Guerrouache, M., Langlois, V., and Tassin, B. (2017). A first overview of textile fibers, including microplastics, in indoor and outdoor environments. Environ. Pollut. *221*, 453–458. https://doi.org/10.1016/j.envpol.2016.12.013.

27. Mai, L., Sun, X.F., Xia, L.L., Bao, L.J., Liu, L.Y., and Zeng, E.Y. (2020). Global riverine plastic outflows. Environ. Sci. Technol. *54*, 10049–10056. https://doi.org/10.1021/acs.est.0c02273.

28. van Sebille, E., Wilcox, C., Lebreton, L., Maximenko, N., Hardesty, B.D., van Franeker, J.A., Eriksen, M., Siegel, D., Galgani, F., and Law, K.L. (2015). A global inventory of small floating plastic debris. Environ. Res. Lett. *10*, 124006. https://doi.org/10.1088/1748-9326/10/12/124006.

29. Cole, M., Lindeque, P., Halsband, C., and Galloway, T.S. (2011). Microplastics as contaminants in the marine environment: a review. Mar. Pollut. Bull. *62*, 2588–2597. https://doi.org/10.1016/j.marpolbul.2011.09.025.

30. Zhang, Y., Wu, P., Xu, R., Wang, X., Lei, L., Schartup, A.T., Peng, Y., Pang, Q., Wang, X., Mai, L., et al. (2023). Plastic waste discharge to the global ocean constrained by seawater observations. Nat. Commun. *14*, 1372. https://doi.org/10.1038/s41467-023-37108-5.

31. Trainic, M., Flores, J.M., Pinkas, I., Pedrotti, M.L., Lombard, F., Bourdin, G., Gorsky, G., Boss, E., Rudich, Y., Vardi, A., and Koren, I. (2020). Airborne microplastic particles detected in the remote marine atmosphere. Commun. Earth Environ. *1*, 64. https://doi.org/10.1038/s43247-020-00061-y.

32. Yang, S., Zhang, T., Gan, Y., Lu, X., Chen, H., Chen, J., Yang, X., and Wang, X. (2022). Constraining microplastic particle emission flux from the ocean. Environ. Sci. Tech. Let. *9*, 513–519. https://doi.org/10.1021/acs.estlett.2c00214.

33. Wong, C.S., Green, D.R., and Cretney, W.J. (1974). Quantitative tar and plastic waste distributions in the pacific ocean. Nature *247*, 30–32. https://doi.org/10.1038/247030a0.

34. Liu, K., Wu, T., Wang, X., Song, Z., Zong, C., Wei, N., and Li, D. (2019). Consistent transport of terrestrial microplastics to the ocean through atmosphere. Environ. Sci. Technol. *53*, 10612–10619. https://doi.org/10.1021/acs.est.9b03427.

35. Lebreton, L.C.M., Van der Zwet, J., Damsteeg, J.W., Slat, B., Andrady, A., and Reisser, J. (2017). River plastic emissions to the world's oceans. Nat. Commun. *8*, 15611. https://doi.org/10.1038/ncomms15611.

36. Stohl, A., Eckhardt, S., Forster, C., James, P., and Spichtinger, N. (2002). On the pathways and timescales of intercontinental air pollution transport. J. Geophys. Res. *107*. ACH 6-1. ACH 6-17. https://doi.org/10.1029/2001jd001396.

37. Leibensperger, E.M., Mickley, L.J., Jacob, D.J., Chen, W.T., Seinfeld, J.H., Nenes, A., Adams, P.J., Streets, D.G., Kumar, N., and Rind, D. (2012). Climatic effects of 1950-2050 changes in US anthropogenic aerosols - Part 1: aerosol trends and radiative forcing. Atmos. Chem. Phys. *12*, 3333–3348. https://doi.org/10.5194/acp-12-3333-2012.

38. Lin, S.J., and Rood, R.B. (1996). Multidimensional flux-form semi-Lagrangian transport schemes. Mon. Weather Rev. *124*, 2046–2070. https://doi.org/10.1175/1520-0493(1996)124<2046:Mffslt>2.0.Co;2.

39. Wu, X., Deng, L., Song, X., and Zhang, G.J. (2007). Coupling of convective momentum transport with convective heating in global climate simulations. J. Atmos. Sci. *64*, 1334–1349. https://doi.org/10.1175/Jas3894.1.

40. Lin, J.T., and McElroy, M.B. (2010). Impacts of boundary layer mixing on pollutant vertical profiles in the lower troposphere: implications to satellite remote sensing. Atmos. Environ. *44*, 1726–1739. https://doi.org/10.1016/j.atmosenv.2010.02.009.

41. Liu, H., Jacob, D.J., Bey, I., and Yantosca, R.M. (2001). Constraints from Pb-210 and Be-7 on wet deposition and transport in a global three-dimensional chemical tracer model driven by assimilated meteorological fields. J. Geophys. Res. *106*, 12109–12128. https://doi.org/10.1029/2000jd900839.

42. Wang, Q., Jacob, D.J., Fisher, J.A., Mao, J., Leibensperger, E.M., Carouge, C.C., Le Sager, P., Kondo, Y., Jimenez, J.L., Cubison, M.J., and Doherty, S.J. (2011). Sources of carbonaceous aerosols and deposited black carbon in the Arctic in winter-spring: implications for radiative forcing. Atmos. Chem. Phys. *11*, 12453–12473. https://doi.org/10.5194/acp-11-12453-2011.

43. Wang, Q., Jacob, D.J., Spackman, J.R., Perring, A.E., Schwarz, J.P., Moteki, N., Marais, E.A., Ge, C., Wang, J., and Barrett, S.R.H. (2014). Global budget and radiative forcing of black carbon aerosol: constraints from pole-to-pole (HIPPO) observations across the Pacific. J. Geophys. Res. Atmos. *119*, 195–206. https://doi.org/10.1002/2013jd020824.

44. Wesely, M.L. (1989). Parameterization of surface resistances to gaseous dry deposition in regional-scale numerical-models. Atmos. Environ. *23*, 1293–1304. https://doi.org/10.1016/0004-6981(89)90153-4.

45. Emerson, E.W., Hodshire, A.L., DeBolt, H.M., Bilsback, K.R., Pierce, J.R., McMeeking, G.R., and Farmer, D.K. (2020). Revisiting particle dry deposition and its role in radiative effect estimates. Proc. Natl. Acad. Sci. USA *117*, 26076–26082. https://doi.org/10.1073/pnas.2014761117.

46. Duncan Fairlie, T., Jacob, D.J., and Park, R.J. (2007). The impact of transpacific transport of mineral dust in the United States. Atmos. Environ. *41*, 1251–1266. https://doi.org/10.1016/j.atmosenv.2006.09.048.

47. Alexander, B., Park, R.J., Jacob, D.J., Li, Q.B., Yantosca, R.M., Savarino, J., Lee, C.C.W., and Thiemens, M.H. (2005). Sulfate formation in sea-salt aerosols: constraints from oxygen isotopes. J. Geophys. Res. *110*, D10307. https://doi.org/10.1029/2004jd005659.

48. Lin, H., Jacob, D.J., Lundgren, E.W., Sulprizio, M.P., Keller, C.A., Fritz, T.M., Eastham, S.D., Emmons, L.K., Campbell, P.C., Baker, B., et al. (2021). Harmonized Emissions Component (HEMCO) 3.0 as a versatile emissions component for atmospheric models: application in the GEOS-Chem, NASA GEOS, WRF-GC, CESM2, NOAA GEFS-Aerosol, and NOAA UFS models. Geosci. Model Dev *14*, 5487–5506. https://doi.org/10.5194/gmd-14-5487-2021.

49. Ginoux, P., Chin, M., Tegen, I., Prospero, J.M., Holben, B., Dubovik, O., and Lin, S.J. (2001). Sources and distributions of dust aerosols simulated with the GOCART model. J. Geophys. Res. *106*, 20255–20273. https://doi.org/10.1029/2000jd000053.

50. Lawrence, P.J., Feddema, J.J., Bonan, G.B., Meehl, G.A., O'Neill, B.C., Oleson, K.W., Levis, S., Lawrence, D.M., Kluzek, E., Lindsay, K., and Thornton, P.E. (2012). Simulating the biogeochemical and biogeophysical

impacts of transient land cover change and wood harvest in the community climate system model (CCSM4) from 1850 to 2100. J. Clim. *25*, 3071–3095. https://doi.org/10.1175/Jcli-D-11-00256.1.

51. Yuan, Z., Pei, C., Li, H., Lin, L., Liu, S., Hou, R., Liao, R., and Xu, X. (2023). Atmospheric microplastics at a southern China metropolis: occurrence, deposition flux, exposure risk and washout effect of rainfall. Sci. Total Environ. *869*, 161839. https://doi.org/10.1016/j.scitotenv.2023.161839.

52. Caracci, E., Vega-Herrera, A., Dachs, J., Berrojalbiz, N., Buonanno, G., Abad, E., Llorca, M., Moreno, T., and Farré, M. (2023). Micro(nano)plastics in the atmosphere of the Atlantic Ocean. J. Hazard Mater. *450*, 131036. https://doi.org/10.1016/j.jhazmat.2023.131036.